Role of hypothalamic MAPK/ERK signaling in diabetes remission induced by the central action of fibroblast growth factor 1

Jenny M. Brown[1,2], Marie A. Bentsen[1,2], Dylan M. Rausch[2], Bao Anh Phan[1], Danielle Wieck[1], Huzaifa Wasanwala[3], Miles E. Matsen[1], Nicole E. Richardson[1], Xin Zhao[4], Peng Zhai[4], Anna Secher[5], Gregory J. Morton[1], Tune H. Pers[2], Michael W. Schwartz[1], and Jarrad M. Scarlett[1,6]

[1] University of Washington Medicine Diabetes Institute, Department of Medicine, Seattle, WA, USA.

[2] University of Copenhagen, Novo Nordisk Foundation Center for Basic Metabolic Research, Copenhagen, Denmark.

[3] University of Central Florida, Department of Medicine, Orlando, FL, USA.

[4] Global Drug Discovery, Novo Nordisk Research China, Beijing, China.

[5] Global Drug Discovery, Novo Nordisk A/S, Maaloev, Denmark.

[6] Department of Pediatric Gastroenterology and Hepatology, Seattle Children's Hospital, Seattle, WA, USA.

Address for Correspondence:

Jarrad M. Scarlett

Jarrad.Scarlett@seattlechildrens.org

University of Washington Medicine Diabetes Institute, Department of Medicine

750 Republican St, F770

Seattle, Washington, 98195, USA.

Phone: (206) 897 5282

Summary

The capacity of the brain to elicit sustained remission of hyperglycemia in rodent models of type 2 diabetes following intracerebroventricular (icv) injection of fibroblast growth factor 1 (FGF1) is well established. Here, we show that following icv FGF1 injection, hypothalamic signaling by extracellular signal-regulated kinases 1 and 2 (ERK1/2), members of the mitogen-activated protein kinase (MAPK) family is induced for at least 24h. Further, we show that in diabetic Lep$^{ob/ob}$ mice, this prolonged response is required for the sustained antidiabetic action of FGF1, since it is abolished by sustained (but not acute) pharmacologic blockade of hypothalamic MAPK/ERK signaling. We also demonstrate that FGF1 R50E, a FGF1 mutant that activates FGF receptors but induces only transient hypothalamic MAPK/ERK signaling, fails to mimic the sustained glucose lowering induced by FGF1. These data identify sustained activation of hypothalamic MAPK/ERK signaling as playing an essential role in the mechanism underlying diabetes remission induced by icv FGF1 administration.

Keywords: Fibroblast growth factor 1, diabetes, brain, hypothalamus, mitogen-activated protein kinase, extracellular signal-regulated kinase

59 **Introduction**

60 Fibroblast growth factor 1 (FGF1) is a prototypical FGF that, in addition to its role
61 in biologic functions ranging from brain development to angiogenesis and wound
62 repair, is implicated the in regulation of feeding and glucose homeostasis[1,2].
63 Recently, FGF1 emerged as a potential antidiabetic agent that following a single
64 intracerebroventricular (icv) injection, induces remission of diabetic hyperglycemia
65 lasting weeks or months in both mouse (Lep$^{ob/ob}$ and LepR$^{db/db}$) and rat (Zucker
66 Diabetic Fatty (ZDF)) models of type-2 diabetes (T2D)[3-6]. Since the effect of icv
67 FGF1 administration to normalize diabetic hyperglycemia in a sustained manner is
68 recapitulated by microinjection of a lower dose of FGF1 directly into mediobasal
69 hypothalamus (MBH), this brain area is implicated as a key target for this sustained
70 antidiabetic response[5]. While recent work points to a role for glia-neuron
71 interactions leading to increased melanocortin signaling[7], as well as to FGF1-
72 induced changes in MBH extracellular matrix[8], the signal transduction mechanisms
73 by which FGF1 action in the MBH induces sustained remission of diabetic
74 hyperglycemia is unknown.

75 Among various intracellular signaling cascades activated by binding of FGF1 to
76 FGF receptors (FGFRs) is the extracellular-signal-regulated kinase (ERK) pathway, a
77 major signaling cassette of the mitogen activated protein kinase (MAPK) signal
78 transduction system that communicates signals arising from activation of cell surface
79 receptors to changes of gene expression occurring in the cell nucleus[9]. Previous work
80 demonstrates that MAPK/ERK signaling is rapidly induced in the hypothalamus of
81 diabetic mice by FGF19, a member of the endocrine FGF family, and that this ERK

82 activation is required for its transient glucose-lowering action[10]. Activation of ERK
83 signaling in the MBH has also been documented following icv administration of FGF1
84 and is associated with robust transcriptional changes related to the ERK pathway in
85 both tanycytes and astrocytes[5,7]. However, neither the role played by ERK signaling
86 in these responses nor the extent to which they contribute to the sustained
87 antidiabetic effect of icv FGF1 is known. The current work was undertaken to
88 address these questions.

89 We report that in diabetic Lep$^{ob/ob}$ mice, the sustained antidiabetic effect of icv
90 FGF1 is abolished by pharmacologic blockade of hypothalamic MAPK/ERK
91 signaling (achieved by central administration of the MAPK inhibitor U0126), but only if
92 this blockade lasts for the 24h duration of FGF1-induced activation of MAPK/ERK
93 signaling in the hypothalamus. We further report that icv injection of FGF1 R50E, a
94 FGF1 mutant that activates FGFRs and induces transient, but not sustained MAPK/ERK
95 signaling[11,12], fails to mimic the sustained diabetes remission induced by icv FGF1
96 administration. We also report transcriptomic evidence pointing to a role for astrocytes
97 (and possibly tanycytes) as primary targets for the hypothalamic response to FGF1.
98 Collectively, these data indicate that durable induction of hypothalamic MAPK/ERK
99 signaling is required for sustained remission of diabetic hyperglycemia induced by
100 icv FGF1 administration and adds to growing evidence of a role for glia-neuron
101 interaction in this response.

102

103 **Results**

104 **Central Administration of FGF1 Induces Sustained ERK1/2 Signaling in the**
105 **Hypothalamus**

106 Consistent with our previous observations in ZDF rats[5], we found using
107 quantitative western blot that in overnight-fasted wild-type (WT) mice,
108 phosphorylation of ERK1/2 (pERK1/2, a biomarker of ERK1/2 activation) was
109 detectable in the hypothalamus within 20 min of icv injection of FGF1 (3 μg), but not
110 following icv vehicle injection (Figure 1A). Since the duration of ERK1/2 activation is
111 a determinant of gene expression and other cellular processes engaged by ERK
112 signaling[13], we next measured the time course of ERK1/2 activation in the
113 hypothalamus following a single icv injection of FGF1. We found that in WT mice,
114 activation of ERK1/2 was readily detected at both the 5h (Figure 1B) and 24h
115 (Figure 1C) time points following icv FGF1 injection, but this response was no
116 longer evident at 48h (Figure 1D). In contrast, changes of hypothalamic pERK1/2
117 content were not observed at any time point after icv vehicle. Interestingly, the
118 magnitude of FGF1-induction of ERK1/2 increased over time, being nearly 3-fold
119 greater at 24h than at 20 min.

120 Next, we sought to compare the degree to which hypothalamic ERK1/2
121 signaling is induced following icv injection of FGF1 to that induced by icv FGF19, an
122 endocrine member of the FGF family that transiently improves systemic glucose
123 metabolism in diabetic rodents[10,14-17]. Prior work has shown that icv FGF19 induces
124 ERK1/2 signaling in the hypothalamus and that improved glucose-tolerance in
125 response to icv FGF19 requires functional ERK1/2 signaling[10]. Acutely, both FGF1
126 and FGF19 rapidly induce activation of ERK1/2 signaling in the MBH following icv

127 injection[5,10], however this effect persisted for 24h only after treatment with FGF1

128 (Figure 1E). Therefore, whereas both FGF1 and FGF19 rapidly activate ERK1/2

129 signaling in the hypothalamus following icv delivery, only FGF1 does so in a manner

130 that is sustained for at least 24h.

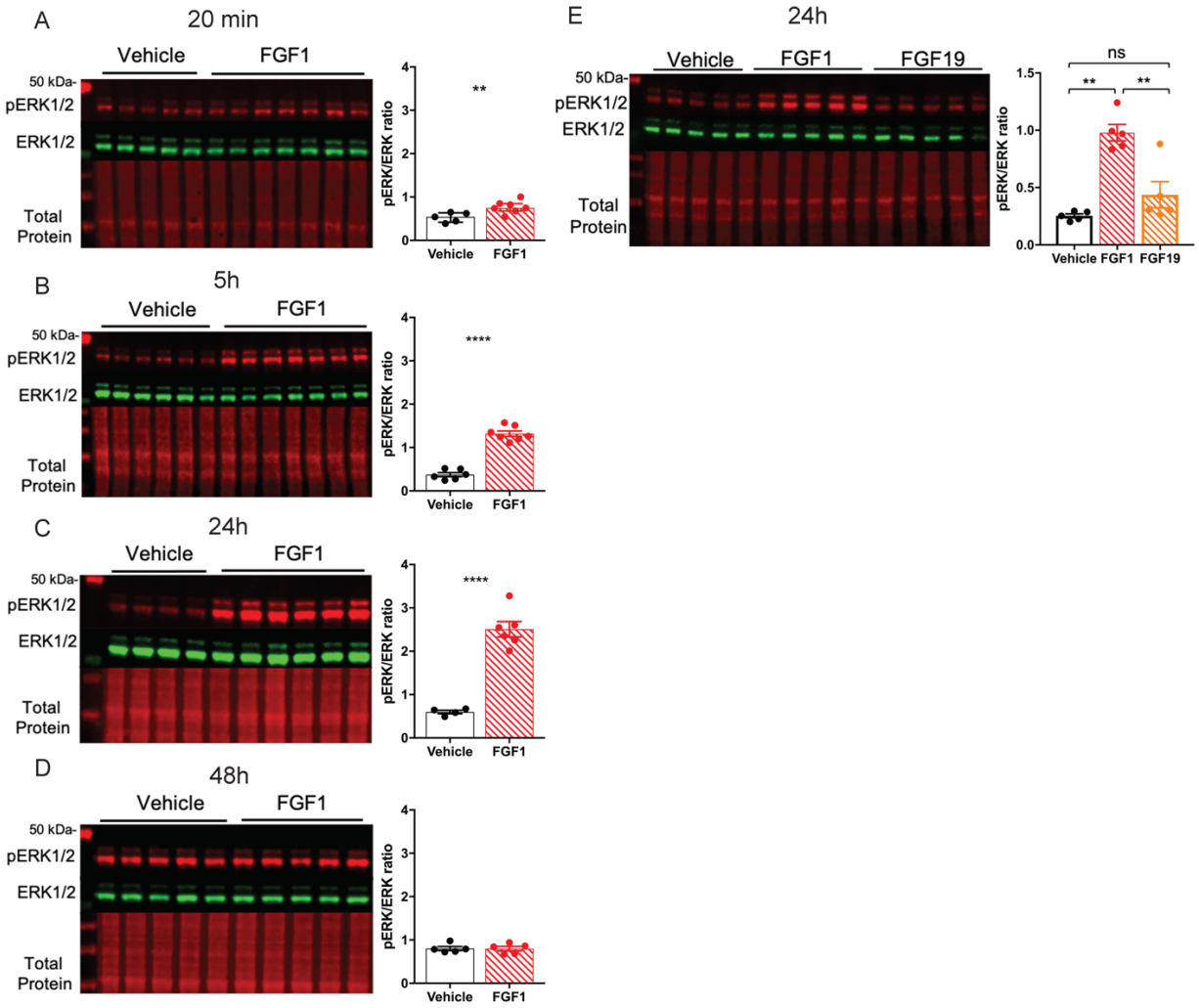

Figure 1- Central Administration of FGF1 Induces Sustained ERK1/2 Signaling in the Hypothalamus. Representative western blot (left panel) and quantitative comparison (right panel) of phosphorylated (red) and total ERK1/2 (green) and total protein (red) from hypothalamic punches from adult male C57Bl6J mice after a single icv injection of either vehicle or FGF1 (3 μg) at **A)** 20 minutes (n=5-7/group, t=3.2497 df=9.8554 p=0.00444) **B)** 5 hours (n=6-7/group, t=11.937 df=10.624 p=8.62e-08) **C)** 24 hours (n=4-6/group, t=10.528, df=5.4845, p=3.816e-05) and **D)** 48 hours (n=5/group, t=-0.0344, df=7.8827, p=0.5133) after injection. pERK1/2 ratio unpaired Welch two sample t-test (one sided). **P<0.01, ****P<0.0001 **E)** Quantitative western

blot of ERK1/2 phosphorylation 24h after a single icv injection of vehicle, FGF1, or FGF19 (n=4-5/group one-way ANOVA $F(2,3.46)=54.83$ $p=0.00241$).

131

132 **Diabetes Remission Induced by Central FGF1 Delivery Requires Functional**

133 **Hypothalamic ERK1/2 Signaling.**

134 To determine whether sustained diabetes remission induced by icv FGF1 in

135 diabetic Lep$^{ob/ob}$ mice requires intact hypothalamic MAPK/ERK signaling, we co-

136 administered the MAPK inhibitor U0126 with FGF1 and measured its impact on

137 both hypothalamic ERK1/2 induction and on the duration of glucose lowering. We

138 found that whereas activation of hypothalamic ERK1/2 signaling following icv

139 administration of FGF1 (3 μg) was acutely blocked by pre-treatment with a single

140 icv injection of U0126 (5 μg) (Figure 2A), this intervention did not prevent FGF1-

141 induced reductions of food intake or body weight, nor did it block sustained lowering

142 of the blood glucose level (Figures 2B–D). To explain this finding, we examined the

143 duration of the effect of icv injection of U0126 (5 μg) on induction of hypothalamic

144 ERK1/2 by icv administration of FGF1 (3 μg). We found that although this U0126

145 pre-treatment regimen was effective early on, it did not attenuate FGF1-induced

146 activation of hypothalamic ERK1/2 at the 24h time point (Figure S1A).

147 This observation prompted us to identify a route, dose, and duration of icv

148 U0126 treatment capable of blocking FGF1-induced ERK1/2 activation for a full 24h

149 period. Whereas neither repeated icv injection of U0126 (Figure S1B) nor

150 continuous infusion of U0126 into the lateral ventricle (Figure S1C) were effective,

151 we asked whether administration into the 3rd ventricle would be more effective,

152 owing to its close proximity to the MBH. Indeed, we found that continuous infusion

153 of U0126 into the 3rd ventricle for 24h (by osmotic mini-pump) following a single
154 intra-3rd ventricular U0126 injection was sufficient to block hypothalamic FGF1-
155 induced ERK1/2 activation for a full 24h (Figure S1C).

156 We therefore employed this 24h 3rd ventricular U0126 administration protocol
157 to investigate the role played by MBH MAPK/ERK1/2 signaling in metabolic
158 responses elicited by icv FGF1 injection (Figure 2E) in diabetic Lep$^{ob/ob}$ mice. We
159 found that whereas this intervention did not prevent initial reductions of food intake,
160 body weight, or blood glucose induced by icv injection of FGF1 (3 μg) (Figures 2F–
161 H), it did prevent sustained remission of diabetic hyperglycemia (Figure 2H).
162 Because our previous work has shown that the initial glucose-lowering effect of icv
163 FGF1 injection is driven primarily by transient anorexia[3,4], a group of vehicle-treated
164 Lep$^{ob/ob}$ mice that were pair-fed to the intake of the group receiving FGF1 was
165 included in this study. Data from this group demonstrates that in animals receiving
166 icv vehicle treatment, pair-feeding to match the reduced food intake induced by icv
167 FGF1 injection was sufficient to lower blood glucose levels initially. However, this
168 glucose-lowering effect was not sustained irrespective of whether pair-feeding was
169 accompanied by icv U0126 or vehicle administration (Figure 2E). Nevertheless, in
170 mice that received both icv FGF1 injection and the 24h U0126 infusion, blood
171 glucose levels returned to their elevated baseline value even before food intake and
172 body weight had done so, whereas glucose levels remained low throughout the
173 duration of the study in mice receiving FGF1 coupled with vehicle instead of U0126
174 (Figures 2E–H). Taken together, these results show that while hypothalamic
175 ERK1/2 activation is not required for the acute, transient effects of icv FGF1 on

176 levels of blood glucose, food intake, or body weight, it is required for sustained

177 remission of diabetic hyperglycemia induced by the central action of FGF1.

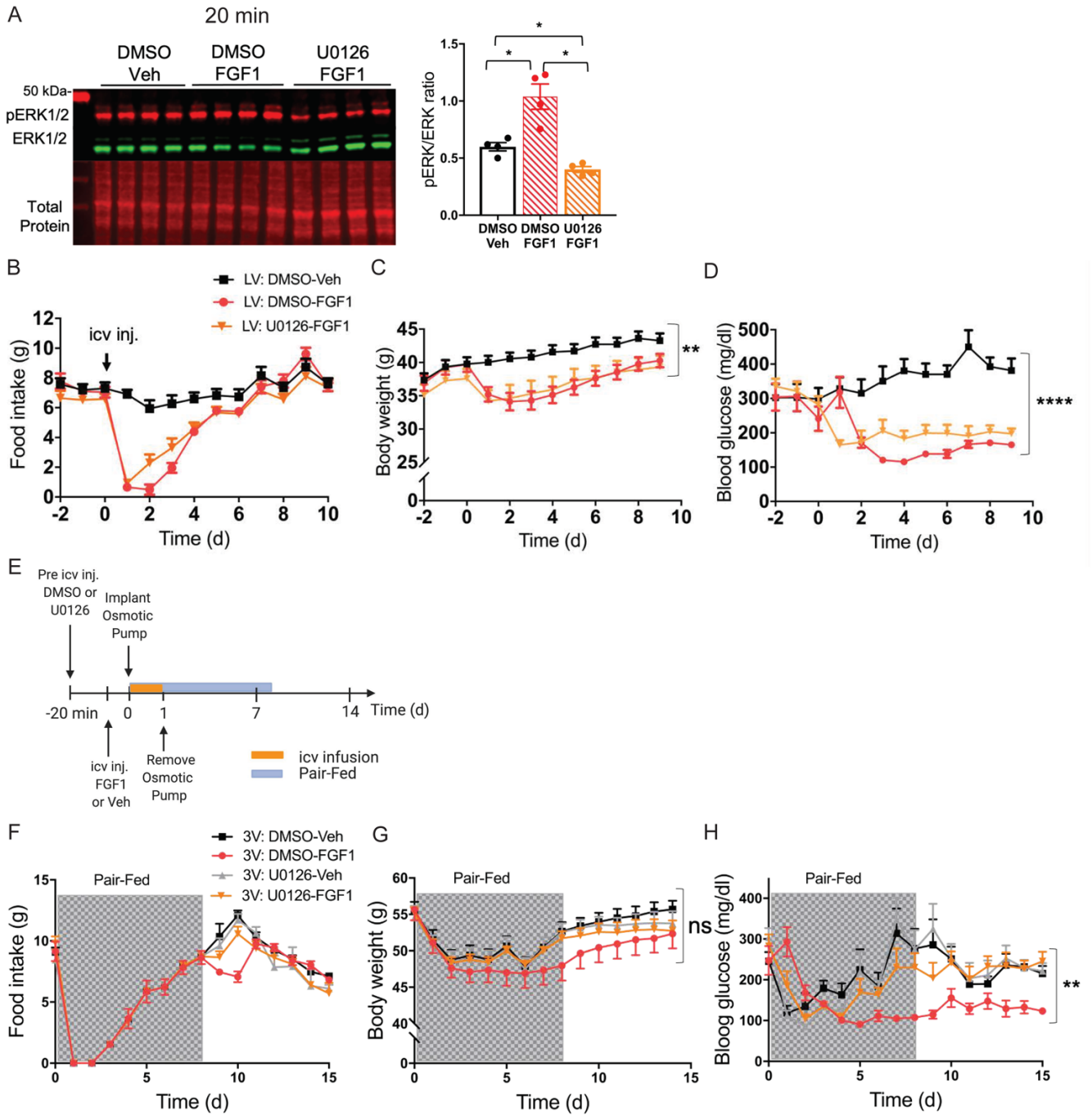

Figure 2- Prolonged MAPK signaling in the MBH is required for diabetes remission induced by central FGF1. A) Representative western blot (left panel) showing phosphorylated (red) and total ERK1/2 (green) and total protein (red), and data quantitation (right panel) from hypothalamic punches from adult male C57Bl6J mice at 20 min after a

injection into the lateral ventricle of the inhibitor of MAPK signaling U0126 (5 μg) or DMSO, followed by injection of either vehicle or FGF1 (n=5/group, one-way ANOVA F(2-5.27)= 20.1692 p=0.00339). Effects of the same treatments on levels of **B)** food intake, **C)** body weight (n=7-8/group; repeated measures nparLD ANOVA.test statistic treatment =4.61 df=1.91 p=0.01) and **D)** blood glucose (n=7-8/group repeated measures nparLD ANOVA.test statistic treatment =27.96 df=1.8 p=7.36e-12) in $Lep^{ob/ob}$ mice. **E)** Strategy for MAPK/ERK inhibition by continuous 3V infusion of U0126 or Vehicle DMSO for 24 hours followed by disconnection of osmotic pump and metabolic phenotyping image created with BioRender.com. Levels of **F)** food intake **G)** Body weight (n=5-8/group repeated measures nparLD ANOVA.test statistic treatment=0.80 df=2.70 p=0.47), and **H)** blood glucose (n=5-8/group repeated measures nparLD ANOVA.test statistic treatment =4.99 df=2.67 p=0.002) measured for 15 days post-treatment with icv injection of either saline vehicle or FGF1 (3ug) followed by a 24h continuous infusion of U0126 or DMSO vehicle into the third ventricle.

The FGF1 Mutant FGF1 R50E Mimics the Effect of Native FGF1 to Rapidly Induce ERK1/2 Activation in the Hypothalamus.

As an alternative test of the hypothesis that diabetes remission induced by icv FGF1 injection requires sustained ERK1/2 activation in the hypothalamus, we repeated these studies in mice using FGF1 R50E, a FGF1 mutant in which arginine at the amino acid position 50 is substituted with glutamate[11]. In cell culture studies, FGF1 R50E retains the ability to bind to and activate FGFRs and induce transient activation of ERK1/2, but the effect is not sustained[11,12,18]. Consistent with these observations, we found that when given at the same dose (3 μg), activation of hypothalamic ERK1/2 by icv injection of FGF1 R50E was comparable to that induced by native FGF1 at the first 3 time points (20 min, 5h and 8h), but no effect was observed at either 14h or 24h after icv injection (Figure 3A). Therefore, FGF1 R50E-induced ERK1/2 activation in the hypothalamus is short-lived in comparison to the more durable response elicited by native FGF1 following icv injection.

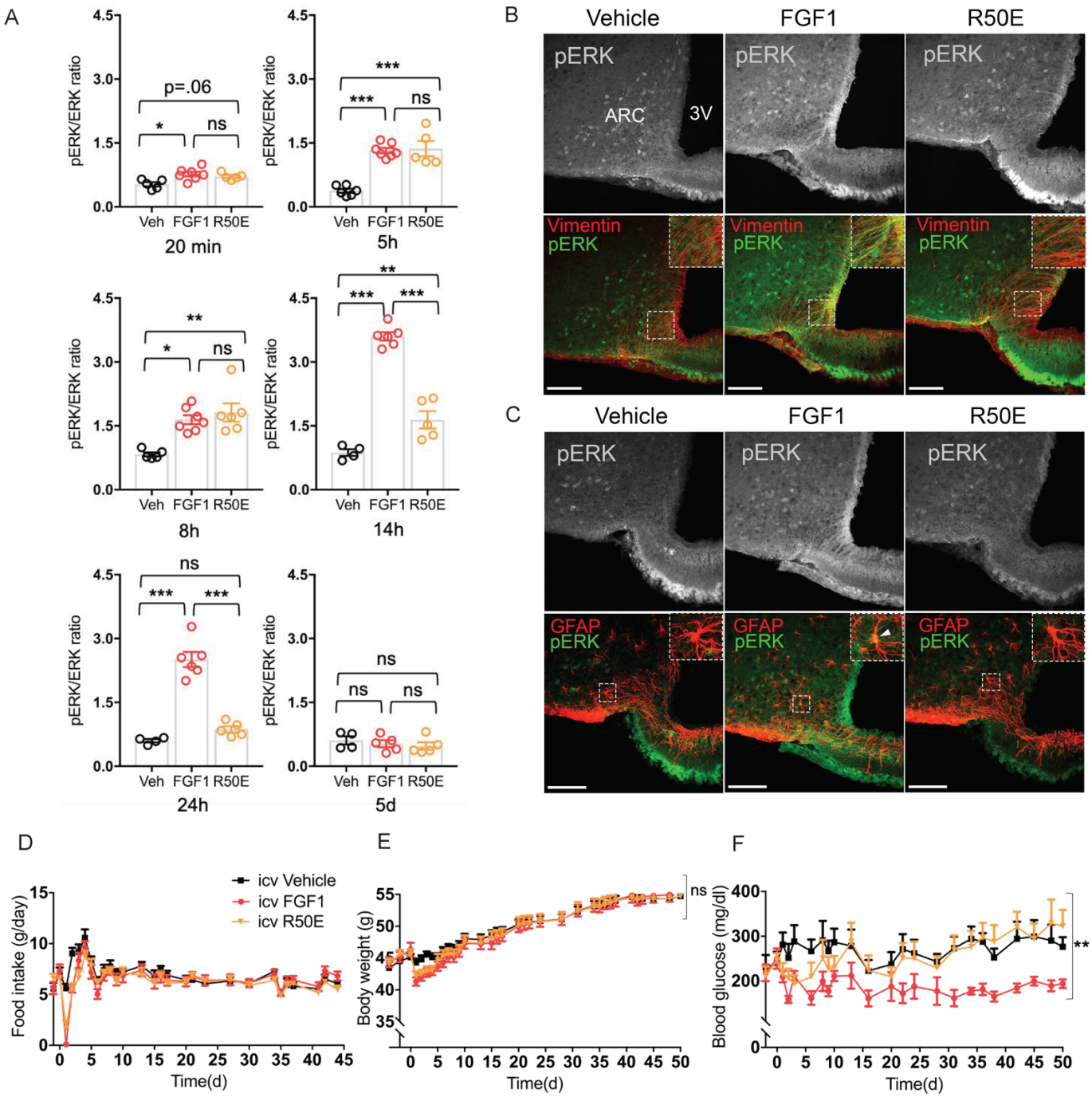

Figure 3- FGF1 Mutant Induces Only Transient ERK1/2 Activation in Hypothalamus and Fails to Induce Sustained Remission of Diabetic Hyperglycaemia. A) Quantitative western blot showing a time course of hypothalamic ERK1/2 phosphorylation after a single icv injection of either vehicle, FGF1 (3µg), or FGF1 R50E (3µg) at the following time points after injection: 20 min (n=5-7/group one-way ANOVA F(2,14)=6.1616 p=0.012); 5h (F(2,15)=31.334 p=4.4e-06) 8h (kruskal-wallis chi-squared=10.361 df=2 p=0.0056); 14h (n=4-6/group F(2,12)=101.94 p=2.95e-08) 24h (F(2,12)=63.339 p=4.17e-07); or 5d (n=4-5/group F(2,11)=0.51 p=0.6) with Tukey's post-

hoc test ns=not significant, **P<0.01, ***P<0.001, ****P<0.0001. **B)** confocal images of the arcuate nucleus (ARC) and third ventricle (3V) showing pERK1/2 (grey) with merged pERK1/2 (green) and vimentin (red) and **C)** pERK1/2 (grey) with merged pERK1/2 (green) and glial fibrillary acidic protein (GFAP) (red) 14h after a single icv injection of either vehicle, FGF1(3µg) or FGF1 R50E (3µg). Scale bar 100 um and inserts representative double-labeled cells. Time course of the effect of the same 3 icv treatments on **D)** food intake, **E)** body weight (n=8-9/group repeated measures nparLD ANOVA.test statistic treatment=0.05 df=1.91 p=0.94), and **F)** plasma glucose levels (n=8-9/group repeated measures nparLD ANOVA.test statistic treatment=5.49 df=1.79 p=0.005) in Lep$^{ob/ob}$ mice.

Based on previous work showing that tanycytes and astrocytes are especially responsive to the effect of icv FGF1 injection to induce sustained ERK1/2 signaling[5,7], we next examined the response of these cell types following icv injection of FGF1 R50E. As anticipated, we observed that compared to icv injection of native FGF1, pERK1/2 induction in both tanycytes (Figure 3B) and astrocytes (Figure 3C) was markedly reduced at the 14h time point after icv injection of FGF1 R50E. These findings confirm that although ERK1/2 signaling is induced in tanycytes and astrocytes following icv administration of either FGF1 or FGF1 R50E, the response to the latter is short-lived compared to the highly durable response to native FGF1.

FGF1 R50E does not Induce Sustained Remission of Diabetic Hyperglycemia.

Having established that unlike native FGF1, the FGF1 R50E mutant does not induce sustained activation of ERK1/2 signaling in the hypothalamus following icv administration, we next sought to determine whether this blunted response corresponds to a reduced ability to induce sustained glucose lowering in diabetic Lep$^{ob/ob}$ mice. We report that in diabetic Lep$^{ob/ob}$ mice, icv injection of FGF1 R50E effectively recapitulated the acute reductions of food intake, body weight, and blood

212 glucose induced by native FGF1 (Figures 3D–F). Whereas icv injection of native
213 FGF1 induced remission of diabetic hyperglycemia that was sustained for at least
214 50 d, consistent with previous reports[3], diabetic Lep$^{ob/ob}$ mice treated icv with FGF1
215 R50E exhibited a complete relapse of hyperglycemia within 14 d of icv injection,
216 coincident with recovery of baseline food intake and body weight (Figures 3D–F).
217 Thus, whereas centrally administered FGF1 R50E mimics the acute but transient
218 effects of native FGF1 on hypothalamic ERK1/2 activation, food intake, weight loss
219 and blood glucose, neither the ERK1/2 activation nor the diabetes remission are
220 sustained in the manner seen with icv FGF1 injection. This set of outcomes
221 effectively replicates what is observed when icv FGF1 is co-administered with the
222 MAPK inhibitor U0126 for 24h, and together these data offer direct evidence that
223 the highly durable antidiabetic action of FGF1 in the brain is dependent on
224 sustained hypothalamic ERK1/2 activation.
225
226 **Transcriptional Analysis of the Hypothalamic Response to Centrally**
227 **administered FGF1 and FGF1 R50E at the Single-Cell Level**
228 To characterize transcriptional differences elicited by sustained versus
229 transient ERK1/2 activation engaged by FGF1, we leveraged a previously
230 unpublished single-cell RNA-sequencing (scRNA-seq) dataset generated as part of
231 a larger study investigating transcriptomic effects of icv injection of FGF1 in the
232 MBH. That unpublished data was generated based on hypothalami from Lep$^{ob/ob}$
233 mice icv injected with FGF1 R50E 5 days prior, and generated simultaneously with
234 the hypothalamic scRNA-seq data from the Lep$^{ob/ob}$ mice icv injected with either

235 FGF1 or vehicle also 5 days prior (Figure 4A)[7]. This analysis revealed that in
236 astrocytes, tanycytes, and oligodendrocyte lineage cells, the effect of icv FGF1
237 injection to induce differentially expressed genes (DEGs; False-discovery rate,
238 FDR<0.05 and $|\log_2$ fold change$|>0.25$) was far greater than was observed following
239 icv injection of the same dose of FGF1 R50E (Figure 4B). Nevertheless, correlation
240 and ranking of differential gene expression by gene (see Methods) revealed that
241 most genes upregulated by FGF1 were also upregulated by FGF1 R50E, but at
242 much lower intensities (Figures 4C-D). From this, we infer that in the hypothalamus
243 of Lep$^{ob/ob}$ mice, transient and sustained ERK activation (induced by icv injection of
244 FGF1 R50E and FGF1, respectively) induce the same gene expression programs
245 but at differing magnitudes. This interpretation is further supported by geneset
246 variation analysis of REACTOME pathways. We found that the majority of
247 'ERK/MAPK' associated pathways showed a significant change in activity,
248 specifically in astrocytes, in response to treatment (Figure 4E). Using weighted
249 gene co-expression network analysis (WGCNA)[19] we further found that gene co-
250 expression modules differed significantly (linear mixed-effects models; FDR<0.05;
251 Supplementary Table 1) between FGF1 and FGF1 R50E treatment in astrocytes,
252 but not other cell types. Specifically, modules ME11 and ME13 were significantly
253 increased in astrocytes from mice receiving FGF1, but not FGF1 R50E, compared
254 to icv vehicle treatment, whereas module ME5 was significantly reduced with FGF1
255 injection, but not with FGF1 R50E. Of interest is that module M13 is significantly
256 enriched (p=0.026) for genes previously reported to be induced upon astrocyte-
257 neuron interaction[20]. These observations support a model in which astrocyte

activation resulting sustained FGF1-induced ERK1/2 signaling favors increased astrocyte-neuron interaction. Whether and how such an effect might induce sustained remission of diabetes is an important unanswered question.

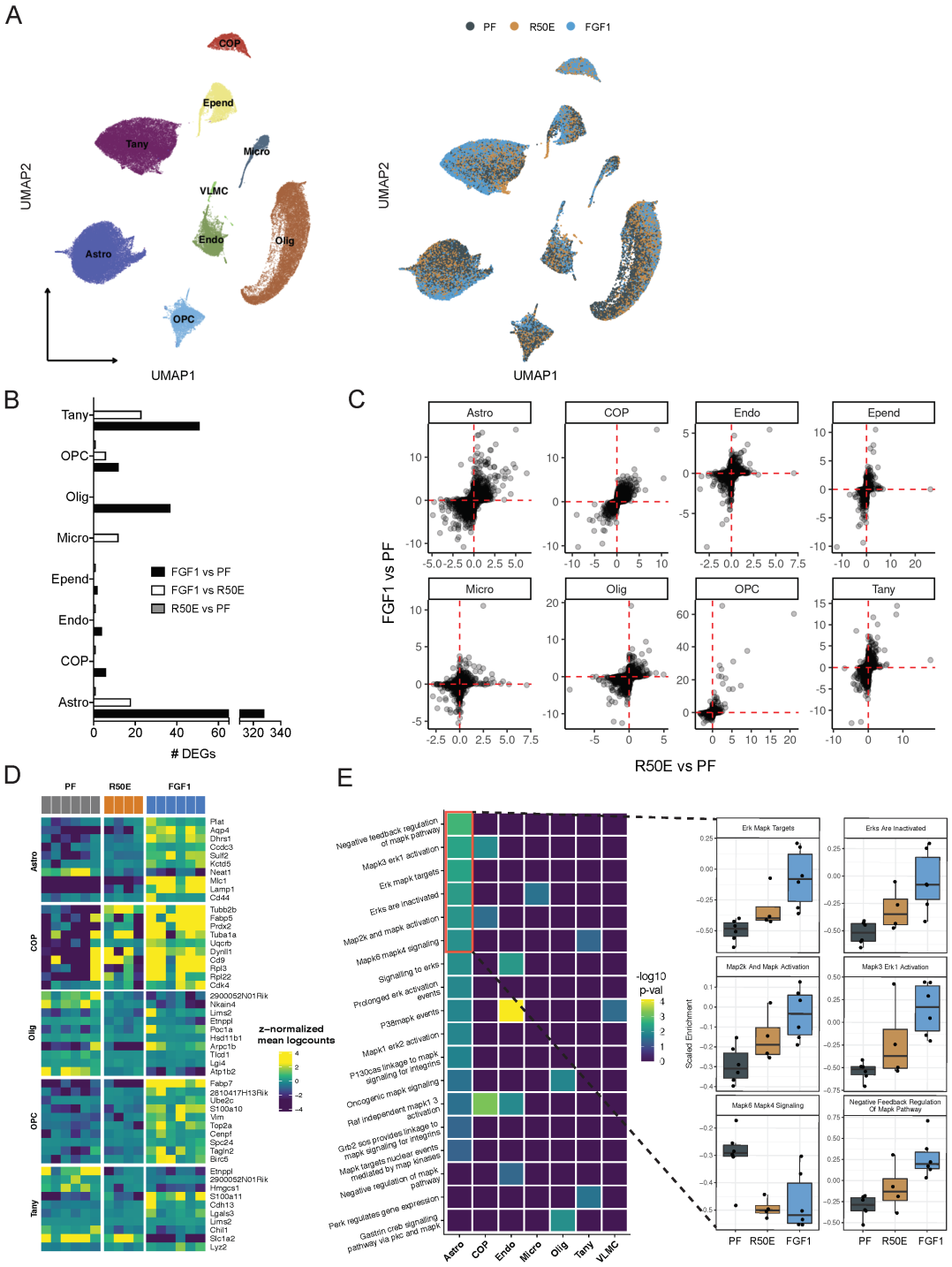

Figure 4- Hypothalamic Single-Cell Transcriptomics Reveal Transcriptional Differences between FGF1 and FGF1 R50E. A) Uniform manifold approximation and projection (UMAP) clustering of hypothalamic glia cells from diabetic Lep$^{ob/ob}$ mice 5 days after a single icv injection of FGF1 or vehicle (GSE153551) or R50E. **B)** Number of differentially expressed genes (DEGs) identified through repeated downsampling (400 cells/group/cell type/iteration: 100 iterations). **C)** Correlation plot of DEGs ranked by |log2 fold change| multiplied with FDR. **D)** Top 10 most upregulated genes by FGF1 compared to pair-fed and FGF1 R50E in selected cell types. **E)** Geneset enrichment analysis of REACTOME terms related to 'MAPK/ERK' targets. Insert: scaled enrichment of top 6 enriched terms by treatment in astrocytes.

Discussion

In the current work, we sought to determine the role played by increased hypothalamic MAPK/ERK signal transduction (measured by pERK1/2 western blot and immunostaining) in the sustained antidiabetic action elicited by icv injection of FGF1 in the Lep$^{ob/ob}$ mouse model of T2D. Our findings demonstrate that *1)* activation of hypothalamic MAPK/ERK signaling is sustained for at least 24h following central administration of FGF1, and *2)* the ability of icv FGF1 injection to induce sustained normalization of diabetic hyperglycemia is dependent on this MAPK/ERK signaling response, but only if it is prolonged. In contrast, hypothalamic MAPK/ERK signaling does not appear to be required for transient effects on food intake, body weight, and blood glucose levels induced by icv FGF1 administration. These findings identify a key role for prolonged hypothalamic MAPK/ERK signaling in the sustained antidiabetic action of FGF1 action in the brain.

MAPK/ERK pathway activation is well documented following the binding of FGFRs by FGF1[9], and a role for hypothalamic ERK signaling in the regulation of glucose homeostasis (in response to administration of leptin, insulin and FGF19) has been reported previously[10,21-23]. Based on these observations, along with our recent

279 work showing that *1)* following icv FGF1 injection, robust induction of ERK1/2 signaling
280 is observed in the hypothalamic arcuate nucleus-median eminence (ARC-ME)[5], and *2)*
281 FGF1 microinjection to this brain area recapitulates sustained glucose lowering
282 observed following icv FGF1 injection[5], we sought to investigate the role of
283 hypothalamic MAPK/ERK signaling in FGF1-induced sustained glucose-lowering. To
284 this end, we first characterized the time course of hypothalamic pERK1/2 induction
285 following icv injection of FGF1 at a dose known to elicit sustained glucose lowering.
286 Consistent with *in vitro* evidence that FGF1 induces both acute and sustained
287 activation of ERK1/2 signaling[13], we report that following a single icv FGF1 injection,
288 hypothalamic pERK1/2 induction is observed within 20 min and persists for a full
289 24h.
290 Our next goal was to determine if this pattern of ERK1/2 activation is required
291 for the sustained antidiabetic effect of icv FGF1, and two separate approaches
292 were employed. First, we administered U0126, a potent and selective inhibitor of
293 MAPK, as a single icv injection prior to icv administration of FGF1. Although this
294 approach proved effective in terms of blocking FGF1-induced ERK1/2 activation in
295 the short-term, MAPK blockade by icv infusion of U0126 over a full 24h period was
296 required to block reversal of diabetic hyperglycemia in response to icv FGF1
297 injection. In contrast, this intervention had no impact on FGF1-induced anorexia,
298 weight loss and associated transient glucose lowering, suggesting that unlike
299 sustained glucose lowering, these responses to icv FGF1 are not dependent on
300 ERK1/2 activation. Collectively, these data suggest that the sustained antidiabetic
301 action of icv FGF1 involves mechanisms distinct from those involved in control of

302 food intake, with the former, but not the latter, being dependent upon sustained
303 ERK1/2 signaling in the hypothalamus.
304 Our second approach to testing this hypothesis took advantage of the fact that
305 while the FGF1 R50E mutant activates FGFRs, it elicits on only transient activation of
306 ERK1/2 in cultured cells[18]. Thus, we predicted that the response to icv injection of the
307 FGF1 R50E mutant would mimic what is observed when the ability of icv FGF1 to
308 induce sustained MAPK/ERK signaling is blocked by central administration of U0126.
309 Indeed, we found that although FGF1 R50E induces hypothalamic ERK1/2 activation
310 following icv injection, the effect is short-lived compared to that induced by icv FGF1
311 injection. Moreover, icv injection of FGF1 R50E fully recapitulated the effects of native
312 FGF1 on food intake, body weight and associated transient amelioration of
313 hyperglycemia, but it failed to induce sustained glucose lowering. Using two
314 complementary approaches, therefore, our findings offer direct evidence that the
315 MAPK/ERK signal transduction mechanism plays a key role in the effect of FGF1 to
316 elicit sustained diabetes remission, while an unrelated signaling pathway mediates
317 FGF1's feeding effects.
318 Relevant to these observations is the mechanism engaged by FGF1-FGFR
319 interaction that leads to sustained MAPK/ERK signal transduction. We suspect a role
320 for integrins, a family of cell adhesion receptors that interact with FGFRs to modulate
321 both receptor activity and the associated intracellular response[11,18,24]. The more
322 durable and robust activation of intracellular signal transduction that results from
323 FGFR-integrin co-activation is implicated in DNA synthesis, cell proliferation, cell
324 migration, and other sustained cellular responses to growth factor signaling[11,25].

325 Integrins are also implicated in the control of insulin sensitivity in peripheral tissues in
326 skeletal muscle and liver[26,27], but not in the regulation of glucose homeostasis by the
327 brain. As the FGF1 R50E mutant was previously characterized (based on work in cell
328 culture) as being unable to activate FGFR1 without engaging integrin signaling, we
329 favor a model in which the latter is induced in the hypothalamus by native FGF1,
330 but not FGF1 R50E, and that this effect is required for sustained ERK1/2
331 activation. Investigation into the contribution made by brain integrin signaling to the
332 antidiabetic effect of FGF1 is a priority for future work.

333 The interpretation of findings reported herein is also informed by recent work that
334 has shed light on how the hypothalamus responds to FGF1. For example, intact
335 hypothalamic melanocortin signaling (determined by interactions between Agrp and
336 Pomc neurons in the ARC) appears to be required for sustained glucose lowering
337 induced by icv FGF1 injection, but is dispensable for acute, transient effects of FGF1
338 on food intake, body weight, and glycemia[7]. In light of our current findings, this work
339 suggests that diabetes remission induced by icv FGF1 involves a MAPK/ERK-
340 dependent mechanism for enhanced melanocortin signaling. Whether this mechanism
341 involves direct effects of FGF1 on Agrp and/or Pomc neurons or instead is mediated
342 via an action on glial cells (*e.g.,* tanycytes or astrocytes) warrants additional study, but
343 the associated finding that FGF1 promotes cellular contacts between astrocytes and
344 Agrp neurons supports the latter possibility[7].

345 Also reminiscent of the current findings is our recent report that hypothalamic
346 perineuronal nets (PNNs, defined as extracellular matrix specializations combined of
347 proteoglycans and hyaluronan), which were recently shown to enmesh neurons in the

348 ARC-ME[28], are also targets for the glucose-lowering action of FGF1. Indeed, PNN
349 formation increases rapidly in the ARC-ME following icv FGF1 injection and, in a rat
350 model of T2D, disruption of this PNN response blocks the sustained antidiabetic action
351 induced by icv FGF1 injection, while having no impact on the acute, transient
352 effects of FGF1 on food intake, body weight, and glycemia[8]. These observations once
353 again parallel those observed when hypothalamic MAPK/ERK signaling either is not
354 induced or is blocked in a sustained manner. As such, they raise the interesting
355 possibility that FGF1-induced stimulation of ARC-ME PNN formation – which likely
356 involves FGF1 action on glial cells – depends upon MAPK/ERK signaling.

357 Additional insight into these possibilities is provided by comparing transcriptional
358 changes occurring in the hypothalamus of Lep$^{ob/ob}$ mice 5 days after icv injection of
359 FGF1 *vs.* FGF1 R50E. While far more DEGs were induced by the former than the latter
360 peptide, a closer examination reveals that the pattern of differential gene expression is
361 in fact similar – what is different is the degree to which genes are induced. When the
362 level of gene expression against known ERK1/2-mediated pathways was interrogated
363 specifically in astrocytes, a similar pattern was detected. Namely, induction of genesets
364 in the ERK1/2 pathway was more robust following icv FGF1 than FGF1 R50E when
365 compared to pair-fed vehicle control mice, but the overall pattern of genesets was
366 similar between the two. Using a different analytic approach, we further found that a co-
367 expressed gene module detected in astrocytes following icv FGF1 injection, one that
368 was not induced by injection of FGF1 R50E, is enriched for genes that are induced
369 when astrocytes are co-cultured with neurons[20]. Although additional studies are needed
370 to establish the role of astrocyte-neuron interaction in the hypothalamic response to

371 FGF1, these data support a model in which sustained ERK1/2 activation initiates a gene
372 co-expression program in astrocytes that allow them to interact with MBH neurons in
373 ways that profoundly impact neurocircuitry involved in controlling glucose homeostasis.
374 We conclude that sustained diabetes remission induced by icv injection of FGF1
375 involves a robust and highly durable MAPK/ERK response in the hypothalamus,
376 whereas the associated transient anorexia and loss of body weight induced by FGF1
377 does not. Although additional work is needed, convergent findings point to a role for
378 prolonged MAPK/ERK signaling in hypothalamic glial cell types as primary targets for
379 the glycemic benefit stemming from FGF1 action in the hypothalamus. Ongoing studies
380 will continue to clarify the role of glia-neuron interactions in the ability of the brain to
381 ameliorate hyperglycemia in a sustained manner in response to FGF1.
382
383
384
385
386
387
388
389
390
391
392
393

394 **Methods**

395 **Resource Availability**

396 **Lead Contact**

397 Further information and requests for resources and reagents should be directed to

398 and will be fulfilled by the Lead Contact Jarrad M. Scarlett

399 (Jarrad.Scarlett@seattlechildrens.org)

400

401 **Materials Availability**

402 This study did not generate new unique reagents

403

404 **Data and Code Availability**

405 The datasets generated during this study are available at NCBI Gene Expression

406 Omnibus (GEO) under Super Series number GSE153551

407 (https://www.ncbi.nlm.nih.gov/geo/query/acc.cgi?acc=GSE153551). Names, references,

408 and version numbers of all software packages used are stated in the Methods section

409 and in the Key Resource Table. Codes are available upon request.

410

411 **Experimental Model and Subject Details**

412 **Animals**

413 Male, 8-week-old C57BL/6J (WT) and Lep$^{ob/ob}$ (B6.Cg-Lep^{ob}/J) mice were

414 purchased from Jackson Laboratory (Bar Harbor, ME) and male, 8-week-old Lep$^{ob/ob}$

415 (B6.V-Lep^{ob}/JRj) were purchased from Janvier Labs, France. All animals were housed

416 individually under specific pathogen-free conditions in a temperature control

417 environment with either a 12 h: 12h or 14 h:10 h light: dark cycle, with 75-80% humidity
418 and ad libitum access to water and standard laboratory chow (LabDiet, St Louis, MO) or
419 Altromin 1310 chow (Brogaarden, Denmark). All animal procedures were performed
420 according to the National Institutes of Health Guide for the Care and Use of Laboratory
421 Animals and approved by the Institutional Animal Care and Use Committee at the
422 University of Washington or performed with approved protocols from The Danish Animal
423 Experiments Inspectorate permit number 2014-15-0201-00181 and the University of
424 Copenhagen project number P16-122.
425
426 **Method Details**
427 **Surgery**
428 Lateral ventricle (LV) and third ventricle (3V) cannulation (8IC315GAS5SC, 26-
429 ga, Plastics One, Roanoke, VA) were performed under isoflurane anesthesia using the
430 following stereotaxic coordinates for mice: LV: -0.7 mm posterior to bregma; 1.3 mm
431 lateral, and 1.3 mm below the skull surface and 3V: -1.8 mm posterior to bregma; mid-
432 line and -4.3 mm below the skull surface. Animals received buprenorphine
433 hydrochloride (Reckitt Benckiser Pharmaceuticals Inc., Richmond, VA) for pain relief
434 and were allowed to recover for one week prior to the study.
435
436 **Icv injections**
437 Mean blood glucose and body weight values were matched between groups
438 before the icv injections. Animals received a single icv injection via the LV of either
439 saline vehicle, recombinant mouse FGF1 (FGF1; Prospect-Tany TechnoGene Ltd., East

440 Brunswick, NJ) dissolved in sterile water at a concentration of 1.5 μg/μl, recombinant
441 human FGF1 (a generous gift from Novo Nordisk) dissolved in PBS pH 6.8, human
442 FGF1 R50E (a generous gift from Novo Nordisk) dissolved in 20 mM Tris pH 8.0, 0.5 M
443 NaCl or human FGF19 (hFGF19; Phoenix Pharmaceuticals, Inc., Burlingame, CA)
444 dissolved in 0.9% normal saline at a concentration of 1.5 μg/μl. and injected using a 33-
445 gauge needle (8IC315IAS5SC, 33 ga, Plastics One, Roanoke, VA) extending 0.8 mm
446 beyond the tip of the icv cannula over 60 s for a final volume of 2 μl[3].
447 To determine if the effect of icv FGF1 administration to induce sustained
448 remission of hyperglycemia in $Lep^{ob/ob}$ mice depends on sustained MAPK/ERK
449 signaling, we studied four groups of diabetic $Lep^{ob/ob}$ mice. Two groups received a single
450 icv injection of FGF1, while the other two received icv vehicle injected into the 3V using
451 a 33-gauge needle (8IC315IAS5SC, 33 ga, Plastics One, Roanoke, VA) extending 1mm
452 beyond the tip of the icv cannula. Each group also received a pre injection and an icv
453 infusion of either the selective MAPK inhibitor U0126 (662005; Millipore Sigma, St.
454 Louis, MO) dissolved in DMSO at a concentration of 30mM or DMSO vehicle 1 μl per
455 hour into the 3V via an micro-osmotic pump (model 1003D; Alzet, Durect Corporation,
456 Cupertino, CA) connected to the 3V cannula for 24 hours.
457
458 **Quantitative western blotting**
459 Hypothalamic punches (3 mm) were collected after indicated treatment.
460 Dissection of a single coronal section (1.5 mm) between the rostral and caudal Circle of
461 Willis using an ice-cold brain matrix followed by a 3 mm biopunch (Harris Uni-Core, Ted
462 Pella Inc, Redding, CA) of the MBH was flash-frozen in liquid nitrogen and stored at -80

463 °C until further processing. Hypothalamic punches were homogenized by sonication in
464 lysis buffer and centrifuged at 10,000 g for 15 minutes supernatant was collected and
465 assayed for protein concentration using a BAC assay. Lysates were mixed in the Licor
466 protein sample loading buffer and heated to 100 °C for 5 minutes. Samples were run on
467 a 10% Bis-Tris criterion XT gel (Bio-Rad Laboratory Inc., Hercules, CA) at 200 volts for
468 25 minutes electrophoretic transferred at 100 V for 45 minutes. Loaded protein
469 concentrations were determined based on primary antibodies 1:1000 rabbit anti-
470 pERK1/2 antibody (#4370; Cell Signaling Technology, Danvers, MA), mouse anti-
471 ERK1/2 (#9107; Cell Signaling Technology, Danvers, MA), secondary IRDye 680RD
472 (#926-68073 Li-cor, Lincoln, NE), IRDye 800CW (#92632212; Li-cor, Lincoln, NE) and
473 total protein Revert 700 Total Protein Stain Kit (#926-11011; Li-cor, Lincoln, NE)
474 combined linear range.
475
476 **Immunofluorescence**
477 Activation of the MAPK/ERK pathway at 14 hours post icv injection pERK1/2 was
478 detected by immunohistochemistry in overnight-fasted C57Bl6J mice. Fourteen hours
479 following icv injection of either vehicle, recombinant FGF1 (3 ug), or FGF1 R50E (3 ug),
480 mice were anesthetized with ketamine and xylazine and perfused with PBS followed by
481 4% paraformaldehyde in 0.1 mol/L PBS, after which brains were removed. Brain were
482 placed in sucrose overnight. Cryostat sectioned (30-um thick) free-floating sections
483 were permeabilized with 0.4% PBS-T overnight Wash in 0.4% PBS-T incubate in
484 pERK1/2 antibody, Host: Rabbit, (#4370;Cell Signaling Technology, Danvers, MA)
485 1:1000 in (3%BSA+0.4%TritonX-100+ 0.2%Normal Donkey Serum in PBS-azide) for

486 24h at 4C Wash sections 5× 10min with 0.4% PBS-T Incubate in Secondary Antibody
487 (DαR 594-A21207) 1:1000 in (3%BSA+0.4%TritonX-100+ 0.2%Normal Donkey Serum
488 in PBS azide) for overnight in 4 C Incubate in DAPI 1:10,000 in PBS for 10min at room
489 temperature and wash tissue 3× 10min with PBS followed by mount, dry and coverslip
490 with PVA mounting media. Immunofluorescence images were captured using a Leica
491 SP8X Scanning Confocal microscope (Leica Microsystems, Buffalo Grove, IL) with an
492 HC FLUOTAR L 25X/0.95 W objective.
493
494 **Generation of single-cell suspensions**
495 Diabetic Lep$^{ob/ob}$ mice received an icv injection of either FGF1 (n=6), FGF1 R50E
496 (n=4) or vehicle (n=6). Mice were euthanized 5 days later, and brains were extracted
497 between 9-12 AM, cooled in ice-cold DMEM/F12 media (Gibco, Thermo Fisher
498 Scientific) for 5 minutes. Brains were then placed ventral surface up into a chilled
499 stainless steel brain matrix and a single coronal section (1.5 mm thick) block was
500 obtained between the rostral and the caudal ends of the Circle of Willis, followed by a
501 triangular section of the MBH using a scalpel. Dissected tissue was digested using the
502 Neural Tissue Dissociation Kit from Miltenyi Biotec (Bergisch Gladbach, Germany) with
503 manual dissociation with the following modifications: sections were immediately placed
504 in preheated (37°C) enzyme mix 1 (1425 ml Buffer X + 37.5 ml Enzyme E) and
505 incubated in closed tubes for 15 minutes at 37 °C under slow, continuous rotation. Then
506 enzyme mix 2 (15 ml Buffer Y + 7.5 ml Enzyme A) was added followed by mechanically
507 dissociated using a wide-tipped, fire-polished Pasteur pipette by pipetting up and down
508 10 times slowly. After a 10-minutes incubation under slow, continuous rotation, using a

509 series of 2 fire-polished Pasteur pipettes with incrementally smaller openings the tissue
510 was gently dissociated until no visible pieces were observed. Cell suspensions were
511 centrifuged at 300xg for 10 minutes at room temperature (RT), and resuspended in 500
512 ml Hanks' Balanced Salt Solution (HBSS) (Gibco, Thermo Fisher Scientific) and 0.04%
513 (w/v) bovine serum albumin (BSA) (Sigma-Aldrich). Following an additional wash
514 (centrifugation at 300xg for 5 minutes and re-suspension in 100 µl HBSS+0.04% BSA)
515 cells were filtered through a 40 mm mesh and 50 ml HBSS+0.04% BSA was added
516 through the filter and transferred to clean tubes. The cell suspension was centrifuged at
517 300xg for 5 minutes and resuspended in 50-150 ml HBSS+0.04% BSA. Cell
518 concentrations were estimated on a NucleoCounter NC-3000 (Chemometec, Denmark)
519 and kept on ice until single-cell encapsulation.
520
521 **Single-cell RNA sequencing**
522 Single-cell cDNA libraries were generated using the 10x Genomics (USA)
523 Chromium single-cell controller and the 3' v2 Reagent Kit according to manufacturer's
524 protocol. Single-cell libraries were sequenced on a NextSeq 500 platform with 3
525 samples on one flow cell to obtain 100 and 32-bp paired end reads using the following
526 read length: read 1, 26 cycles, read 2, 98 cycles and i7 index, 8 cycles.
527
528 **Single-cell RNA-sequencing data processing**
529 Cell Ranger version 1.2 (10x Genomics, USA) was used to de-multiplex and
530 quantify unique molecular identifiers (UMI). A count matrix was generated for each
531 sample with default parameters and genes were mapped to the mouse reference

532 genome GRCm38 (mm10, part of the Cell Ranger software package; for the scRNA-seq
533 dataset) or an adapted reference from the mouse reference genome including introns
534 (for the snRNA-seq dataset), following the steps outlined on the 10x Genomics website
535 (https://support.10xgenomics.com/single-cell-gene
536 expression/software/pipelines/latest/advanced/references#premrna). Barcodes were
537 filtered to include those with a total UMI count >10% of the 99th percentile of the
538 expected recovered cells. Next, Scrublet[29] was run with default parameters to identify
539 likely doublets which were subsequently removed from the expression matrix. Further
540 processing was performed using the Seurat[30,31] R package (version 2.3). Cells in which
541 <400 or >4,000 expressed genes were detected, as well any cell with >20%
542 mitochondrial and/or ribosomal transcripts were discarded. Counts were normalized
543 using the SCtransform() function from Seurat. Variable genes were identified using the
544 FindVariableGenes() function with default settings. Unwanted sources of variation, e.g.
545 number of UMIs and ribosomal and mitochondrial percentage, were regressed out using
546 the ScaleData() function. Principal components were identified with variable genes
547 using the RunPCA() function. The PCs for clustering were identified using the
548 maxLikGlobalDimEst function from the intrinsicDimension[32] package which is described
549 as best practice[33]. These 10 PCs were used to identify clusters and with the
550 FindClusters() function at a resolution of 0.2. All neuronal lineage cells were removed
551 from this dataset, as the quality was poor due to mouse age (myelination/neuron
552 fragility).
553 This dataset was then merged with the previously published part of this dataset
554 comprising of hypothalamic cells from vehicle and FGF1 treated mice. As cells merged

555 into the expected clusters, no integration methods were required. Cluster labels from
556 the previous dataset were used to annotate the clusters found in the merged dataset.
557 The final step was to further remove any artifacts/doublets, which had been
558 missed in the initial round of processing. Each cell type underwent a round of iterative
559 clustering as described above. Within each cell type, any cluster in which 50% of cells
560 originated from a single sample was removed. The FindMarkers() function was used to
561 identify markers of each subcluster, which were removed if enriched for marker genes
562 of a different cell type.
563 Finally, for each cell, the silhouette index, a measure quantifying the similarity of
564 a given cell to its assigned cluster compared to other clusters, was computed, and
565 subsequently in order to remove cells that could not confidently be assigned to a single
566 cluster, cells with a negative silhouette index were discarded.
567
568 **Single-cell RNA-sequencing analyses**
569 Cell Type Abundance
570 Cell type abundance per individual sample was calculated by summing the total number
571 of cells within each defined cell cluster and then dividing by the total number of cells
572 collected per sample. Shifts in cell type abundance across conditions were tested using
573 a mixed effects linear model with a random effect for samples to account for the
574 hierarchical structure of the data.
575
576 Differential State analysis

577 Using the Muscat package() pre-defined clusters were split by sample requiring at least
578 10 cells per sample-cluster combination[34]. Raw counts were summed across each
579 gene-sample-cluster combination to generate a single column per sample-cluster. This
580 matrix was then fed directly into edgeR() for standard processing[35]. A gene was
581 considered differentially expressed if the adjusted local p-value (adjusted within a
582 cluster) was less than 0.05.
583
584 Correlation Analysis
585 Following DGE analysis, each gene was assigned a rank within each cluster treatment
586 combination based on its differential expression (-log10(p-value) * log2FoldChange).
587 The transcriptomic response to the multiple treatment paradigms were then compared
588 to one another by calculating the spearman's correlation of gene rankings.
589
590 GSVA analysis
591 Gene set variation analysis was performed using the R package `GSVA` function with
592 default parameter s(method="gsva")[36]. GSVA implements a non-parametric
593 unsupervised method for gene set enrichment that transforms the data from a gene by
594 sample matrix to a gene-set by sample matrix, allowing for individual sample gene-set
595 enrichment testing. As input to GSVA, we calculated the pseudobulk profiles from each
596 sample cluster combination which were then normalized with the variance stabilizing
597 transformation function from DESeq2. All gene sets from the REACTOME database
598 were tested for enrichment. The association between gene set enrichment and
599 treatment status was assessed using linear regression. A linear model with the

600 normalized enrichment score as dependent and treatment group as independent
601 variable was constructed for each gene set. P-values were adjusted for multiple testing
602 using the FDR correction.
603
604 WGCNA and adjacency matrix calculation
605 The WGCNA package (version 1.66) (cite number 17) implemented in R was used[37].
606 Pearson correlation coefficient was used for the single-cell data and signed network
607 parameter was used to compute the gene-gene adjacency matrix. Powers
608 corresponding to the top 95th percentile of network connectivity or above were
609 discarded and the lowest soft threshold power between 1 and 30 to achieve a scale-free
610 topology R-squared fit of 0.8 was selected.
611
612 WGCNA hierarchical clustering
613 The topological overlap matrices were converted to distance matrices, and the hclust()
614 function was used with the complete method to cluster genes hierarchically. The
615 cutreeDynamic() function was used with a deepSplit parameter of 2 and the pamStage
616 parameter set to FALSE to carve the dendrogram into modules with at least 15 genes.
617 The moduleEigengenes() function was used to compute module eigengenes, the vector
618 of cell embeddings on the first PC of each module's expression submatrix. The
619 mergeCloseModules() function was used to merge modules, using a cutHeight of ≤0.2,
620 corresponding to a Pearson correlation between module eigengenes of ≥0.8. The
621 module eigengenes and expression matrices were used with the signedKME() function
622 to compute gene–module Pearson correlations, or kMEs, a measure of how close each

623 gene is to each module. Module treatment associations were tested using a linear
624 mixed-effects model with the lme4 R package[38] (function lmer()), using a random effect
625 for each sample. Significance values are FDR corrected to account for multiple testing.
626
627 Astrocyte Enrichment
628 To characterize WGCNA modules found enriched in FGF1 treated astrocytes
629 when compared to FGF1-R50E and vehicle treated mice, a hypergeometric enrichment
630 test was performed using markers of astrocytes in middle cerebral artery occlusion
631 (MCAO)/lipopolysaccharide (LPS) mice or astrocytes co-cultured with neurons. Prior to
632 the analysis, the (GSE35338) [39] and (E-MTAB-5514) [20] datasets were downloaded and
633 DEG analysis was performed. Genesets were constructed by identifying any gene with
634 a $\log_2$ fold-change>2 and FDR<0.05 (omitted for the GSE35338[39] dataset) in any of the
635 conditions described. Any genes shared between LPS and MCAO at Day 1 were
636 assigned to the PAN-reactive geneset. Furthermore, any gene found to overlap
637 between LPS and MCAO was removed from the geneset. All p-values were FDR-
638 corrected using sBH correction.
639
640 **Statistical Analysis**
641 Data from individual experiment are shown as dot plots representing data from
642 individual animals and bar graphs representing average ±SEM. Statistical analyses
643 were performed using R [40]. Student's t-test was used to compare the means in two
644 groups and one-way ANOVA to compare three groups assumptions of test were
645 satisfied. For data that was collected repeatedly on each individual animal overtime we

646 employed robust non-parametric methodology statistical procedures to enable accurate
647 and reliable analysis of longitudinal measurements with minimal conditions and have
648 competitive performance for small sample size when (semi)parametric assumptions
649 were are not satisfied. Longitudinal data were analyzed using a linear mixed model
650 including fixed effect of treatment and day and random effects of animal. Linear mixed
651 models were conducted with the R statistical package "nlme"[41], or the equivalent
652 nonparametric test using the R statistical package "nparLD" [42] and followed up by post
653 hoc analysis using nparcomp[43]. Probability values less than 0.05 were considered
654 statistically significant.
655

656 **Acknowledgements**

657 The authors are grateful for the technical assistance provided Helle Kinggaard Lilja-
658 Fischer, Cecilia Ratner, Birgitte Holst, and the Single-cell Omics Platform at the Novo
659 Nordisk Foundation Center for Basic Metabolic Research, University of Copenhagen.
660 The authors thank Nathanial Peters at the University of Washington Keck Imaging
661 Center for technical assistance and the National Institutes of Health (S10-OD-016240)
662 for support to the W.M. Keck Foundation Center for Advanced Studies in Neural
663 Signaling. JMB was supported by National Heart, Lung, and Blood Institute T32 training
664 grant HL-007312 and the Diabetes Research Center Samuel and Althea Stroum
665 Endowed Graduate Fellowship and HW was supported by the NIDDK-funded Diabetes,
666 Obesity and Metabolism Training Grant (T32 DK007247) at the University of
667 Washington. This work was supported by NIH-NIDDK grants: K08DK114474 (JMS),
668 R01DK101997 (MWS), R01DK089056 (GJM), R01DK083042 (GJM and MWS) and an

American Diabetes Association Innovative Basic Science Award (ADA 1-19-IBS-192; GJM). This work was also supported by the NIH-NIDDK–funded Nutrition Obesity Research Center (NORC; P30DK035816) and the Diabetes Research Center (DRC; P30DK017047) at the University of Washington. Additional funding to support these studies was provided to JMS by the UW Royalty Research Fund (RRF; A139339) and to THP by the Lundbeck Foundation (Grant number R190-2014-3904). Funding was also provided to MWS by Novo Nordisk (CMS-431104) and to MAB by the Novo Nordisk Foundation (NNF17OC0024328) and the Novo Nordisk Foundation Center for Basic Metabolic Research, which is an independent research center at the University of Copenhagen partially funded by an unrestricted donation from the Novo Nordisk Foundation (NNF10CC1016515).

Author Contributions

JMB, MWS, and JMS conceived the project. JMB, MAB, THP, MWS, and JMS designed the experiments. JMB, MAB, DMR, BAP, DW, HW, MEM, NER and JMS, performed the experiments. JMB, MAB, DMR, BAP, XZ, PZ, AS, GJM, THP, MWS, and JMS acquired, analyzed, and interpreted the data. JMB, MAB, DMR, MWS, and JMS drafted and revised the manuscript. All authors approved the final version of the manuscript. JMS is the guarantor of this work and, as such, had full access to all of the data in the study and takes responsibility for the integrity of the data and the accuracy of the data analysis.

692 **Duality of Interest.**

693 Funding in support of these studies was provided to MWS by Novo Nordisk A/S (CMS-

694 431104). No other potential conflicts of interest relevant to this article were reported.

695

696 **References**

697

698 1 Zakrzewska, M., Marcinkowska, E. & Wiedlocha, A. FGF-1: From Biology Through
699 Engineering to Potential Medical Applications. *Critical Reviews in Clinical Laboratory*
700 *Sciences* **45**, 91-135, doi:10.1080/10408360701713120 (2008).
701 2 Suh, J. M. *et al.* Endocrinization of FGF1 produces a neomorphic and potent insulin
702 sensitizer. *Nature* **513**, 436-439, doi:10.1038/nature13540 (2014).
703 3 Scarlett, J. M. *et al.* Central injection of fibroblast growth factor 1 induces sustained
704 remission of diabetic hyperglycemia in rodents. *Nature Medicine* **22**, 800-806,
705 doi:10.1038/nm.4101 (2016).
706 4 Scarlett, J. M. *et al.* Peripheral Mechanisms Mediating the Sustained Antidiabetic Action
707 of FGF1 in the Brain. *Diabetes* **68**, 654, doi:10.2337/db18-0498 (2019).
708 5 Brown, J. M. *et al.* The Hypothalamic Arcuate Nucleus–Median Eminence Is a Target for
709 Sustained Diabetes Remission Induced by Fibroblast Growth Factor 1. *Diabetes* **68**,
710 1054-1061, doi:10.2337/db19-0025 (2019).
711 6 Tennant, K. G., Lindsley, S. R., Kirigiti, M. A., True, C. & Kievit, P. Central and
712 Peripheral Administration of Fibroblast Growth Factor 1 Improves Pancreatic Islet Insulin
713 Secretion in Diabetic Mouse Models. *Diabetes* **68**, 1462-1472, doi:10.2337/db18-1175
714 (2019).
715 7 Bentsen, M. A. *et al.* Transcriptomic analysis links diverse hypothalamic cell types to
716 fibroblast growth factor 1-induced sustained diabetes remission. *Nature Communications*
717 **11**, 4458, doi:10.1038/s41467-020-17720-5 (2020).
718 8 Alonge, K. M. *et al.* Hypothalamic perineuronal net assembly is required for sustained
719 diabetes remission induced by fibroblast growth factor 1 in rats. *Nat Metab*,
720 doi:10.1038/s42255-020-00275-6 (2020).
721 9 Raju, R. *et al.* A Network Map of FGF-1/FGFR Signaling System. *J Signal Transduct*
722 **2014**, 962962, doi:10.1155/2014/962962 (2014).
723 10 Marcelin, G. *et al.* Central action of FGF19 reduces hypothalamic AGRP/NPY neuron
724 activity and improves glucose metabolism. *Mol Metab* **3**, 19-28,
725 doi:10.1016/j.molmet.2013.10.002 (2014).
726 11 Mori, S. *et al.* Direct binding of integrin alphavbeta3 to FGF1 plays a role in FGF1
727 signaling. *J Biol Chem* **283**, 18066-18075, doi:10.1074/jbc.M801213200 (2008).
728 12 Mori, S. *et al.* A dominant-negative FGF1 mutant (the R50E mutant) suppresses
729 tumorigenesis and angiogenesis. *PLoS One* **8**, e57927,
730 doi:10.1371/journal.pone.0057927 (2013).
731 13 Marshall, C. J. Specificity of receptor tyrosine kinase signaling: transient versus
732 sustained extracellular signal-regulated kinase activation. *Cell* **80**, 179-185,
733 doi:10.1016/0092-8674(95)90401-8 (1995).
734 14 Morton, G. J. *et al.* FGF19 action in the brain induces insulin-independent glucose
735 lowering. *J Clin Invest* **123**, 4799-4808, doi:10.1172/JCI70710 (2013).

15 Perry, R. J. *et al.* FGF1 and FGF19 reverse diabetes by suppression of the hypothalamic-pituitary-adrenal axis. *Nat Commun* **6**, 6980, doi:10.1038/ncomms7980 (2015).
16 Lan, T. *et al.* FGF19, FGF21, and an FGFR1/beta-Klotho-Activating Antibody Act on the Nervous System to Regulate Body Weight and Glycemia. *Cell Metab* **26**, 709-718 e703, doi:10.1016/j.cmet.2017.09.005 (2017).
17 Fu, L. *et al.* Fibroblast growth factor 19 increases metabolic rate and reverses dietary and leptin-deficient diabetes. *Endocrinology* **145**, 2594-2603, doi:10.1210/en.2003-1671 (2004).
18 Yamaji, S. *et al.* A novel fibroblast growth factor-1 (FGF1) mutant that acts as an FGF antagonist. *PLoS One* **5**, e10273, doi:10.1371/journal.pone.0010273 (2010).
19 Langfelder, P. & Horvath, S. WGCNA: an R package for weighted correlation network analysis. *BMC Bioinformatics* **9**, 559, doi:10.1186/1471-2105-9-559 (2008).
20 Hasel, P. *et al.* Neurons and neuronal activity control gene expression in astrocytes to regulate their development and metabolism. *Nat Commun* **8**, 15132, doi:10.1038/ncomms15132 (2017).
21 Balland, E. *et al.* Hypothalamic tanycytes are an ERK-gated conduit for leptin into the brain. *Cell Metab* **19**, 293-301, doi:10.1016/j.cmet.2013.12.015 (2014).
22 Mayer, C. M. & Belsham, D. D. Insulin directly regulates NPY and AgRP gene expression via the MAPK MEK/ERK signal transduction pathway in mHypoE-46 hypothalamic neurons. *Mol Cell Endocrinol* **307**, 99-108, doi:10.1016/j.mce.2009.02.031 (2009).
23 Zhang, J. *et al.* ERK1/2 mediates glucose-regulated POMC gene expression in hypothalamic neurons. *J Mol Endocrinol* **54**, 125-135, doi:10.1530/JME-14-0330 (2015).
24 Desgrosellier, J. S. & Cheresh, D. A. Integrins in cancer: biological implications and therapeutic opportunities. *Nat Rev Cancer* **10**, 9-22, doi:10.1038/nrc2748 (2010).
25 Latko, M. *et al.* Cross-Talk between Fibroblast Growth Factor Receptors and Other Cell Surface Proteins. *Cells* **8**, 455, doi:10.3390/cells8050455 (2019).
26 Kang, L. *et al.* Integrin-Linked Kinase in Muscle Is Necessary for the Development of Insulin Resistance in Diet-Induced Obese Mice. *Diabetes* **65**, 1590-1600, doi:10.2337/db15-1434 (2016).
27 Williams, A. S. *et al.* Integrin-Linked Kinase Is Necessary for the Development of Diet-Induced Hepatic Insulin Resistance. *Diabetes* **66**, 325-334, doi:10.2337/db16-0484 (2017).
28 Mirzadeh, Z. *et al.* Perineuronal net formation during the critical period for neuronal maturation in the hypothalamic arcuate nucleus. *Nature Metabolism* **1**, 212-221, doi:10.1038/s42255-018-0029-0 (2019).
29 Wolock, S. L., Lopez, R. & Klein, A. M. Scrublet: Computational Identification of Cell Doublets in Single-Cell Transcriptomic Data. *Cell Syst* **8**, 281-291.e289, doi:10.1016/j.cels.2018.11.005 (2019).
30 Butler, A., Hoffman, P., Smibert, P., Papalexi, E. & Satija, R. Integrating single-cell transcriptomic data across different conditions, technologies, and species. *Nature Biotechnology* **36**, 411-420, doi:10.1038/nbt.4096 (2018).
31 Stuart, T. *et al.* Comprehensive Integration of Single-Cell Data. *Cell* **177**, 1888-1902.e1821, doi:10.1016/j.cell.2019.05.031 (2019).
32 Johnsson, K., Soneson, C. & Fontes, M. Low Bias Local Intrinsic Dimension Estimation from Expected Simplex Skewness. *IEEE Transactions on Pattern Analysis and Machine Intelligence* **37**, 196-202, doi:10.1109/TPAMI.2014.2343220 (2015).
33 Germain, P.-L., Sonrel, A. & Robinson, M. D. pipeComp, a general framework for the evaluation of computational pipelines, reveals performant single cell RNA-seq preprocessing tools. *Genome Biology* **21**, 227, doi:10.1186/s13059-020-02136-7 (2020).

34 Crowell, H. L. *et al.* muscat detects subpopulation-specific state transitions from multi-sample multi-condition single-cell transcriptomics data. *Nature Communications* **11**, 6077, doi:10.1038/s41467-020-19894-4 (2020).
35 Robinson, M. D., McCarthy, D. J. & Smyth, G. K. edgeR: a Bioconductor package for differential expression analysis of digital gene expression data. *Bioinformatics* **26**, 139-140, doi:10.1093/bioinformatics/btp616 (2009).
36 Hänzelmann, S., Castelo, R. & Guinney, J. GSVA: gene set variation analysis for microarray and RNA-Seq data. *BMC Bioinformatics* **14**, 7, doi:10.1186/1471-2105-14-7 (2013).
37 Langfelder, P. & Horvath, S. WGCNA: an R package for weighted correlation network analysis. *BMC Bioinformatics* **9**, 559, doi:10.1186/1471-2105-9-559 (2008).
38 Bates, D., Mächler, M., Bolker, B. & Walker, S. Fitting Linear Mixed-Effects Models Using lme4. *2015* **67**, 48, doi:10.18637/jss.v067.i01 (2015).
39 Zamanian, J. L. *et al.* Genomic Analysis of Reactive Astrogliosis. *The Journal of Neuroscience* **32**, 6391-6410, doi:10.1523/jneurosci.6221-11.2012 (2012).
40 R: A Language and Environment for Statistical Computing (Vienna, Austria, 2013).
41 Jose Pinheiro, D. B., Saikat DebRoy, Deepayan Sarkar, and R Core Team. nlme: Linear and Nonlinear Mixed Effects Models. (2013).
42 Konietschke, K. N. a. Y. R. G. a. E. B. a. F. nparLD: An R Software Package for the Nonparametric Analysis of Longitudinal Data in Factorial Experiments. *Journal of Statistical Software* **50**, 1-23 (2012).
43 Konietschke, F., Placzek, M., Schaarschmidt, F. & Hothorn, L. A. nparcomp: An R Software Package for Nonparametric Multiple Comparisons and Simultaneous Confidence Intervals. *2015* **64**, 17, doi:10.18637/jss.v064.i09 (2015).